Demonstration of a 40Gbps Bi-directional Air-to-Ground Millimeter Wave Communication Link

Qi Tang[#1], Abhishek Tiwari[#], Inigo del Portillo[#], Michael Reed[#], Hongyu Zhou[#], Dudi Shmueli[#], Gunnar Ristroph[*], Steven Cashion[#], Dawei Zhang[#], Joseph Stewart[#], Pratheep Bondalapati[#], Qi Qu[#], Yan Yan[#], Bob Proctor[#], Hamid Hemmati[#]

[#]*Facebook Connectivity, 1 Hacker Way, Menlo Park, CA United States*

[*]*IJK Controls, South Pasadena, CA United States*

[1]qitang@fb.com

***Abstract*— We describe the design, development, and field demonstration of a high-throughput E-band communication link between a ground station and a Cessna aircraft flying at an altitude of 7km and a top speed of 463km/h. The link achieved a peak data rate of 40Gbps bi-directional (80Gbps combined simultaneously), and robustly maintained a sustained data rate of 40 Gbps in downlink and 36Gbps in uplink direction for the 12km air-to-ground slanted path. The average power consumption of the flight terminal prototype was measured at 363 Watts in average, and mass at 11.8kg. We also report the results of a test campaign in Quillayute, WA to spot-check the ITU models for rain and cloud attenuation over an air-to-ground link. Using the proven system performance and ITU path loss models, we show that the terminal could be used to provide the maximum bidirectional 40Gbps data rates up to an altitude of 28km and 10Gbps up to 310km. To the best of the authors' knowledge, the very high capacity (> 10Gbps in each direction) millimeter wave communication link system between a ground station and a fast-moving aerial platform over significant ranges (> 10km slanted range) is a world first.**

***Keywords*—Air-to-ground, Rural Connectivity, E-band, High Altitude Platform, Millimeter Wave, Pointing Acquisition and Tracking, UAV**

I. Introduction

High Altitude Platforms (HAP) and Low Earth Orbit (LEO) satellite constellations have been increasingly gaining in popularity, as they are envisioned as enabling technologies to provide broadband internet access in remote rural areas [1]. To make these technologies economically viable, high-throughput long-range wireless communication links are needed to connect the HAPs or satellites to fiber Points-of-Presence on the ground. However, delivering such links presents many challenges, as they need the following attributes: (1) High capacity – able to serve as backhaul for multiple ground-based radio access networks; (2) Long range – HAPs fly at an altitude of 20-30km and LEO satellites orbit in the 500-1200km range; (3) Low size, weight and power (SWaP) of the flight terminal; (4) High accuracy in pointing, acquisition, and tracking (PAT); (5) Ability to maintain the link in the presence of high-speed flight terminal motion and vibration; (6) High link availability under different weather conditions; (7) Compensation for Doppler spread in the channel.

We introduce a brief survey of demonstrated high-capacity (>10Gbps) and long-range (>10km) wireless communication links in recent years. All systems have used either free-space optics, millimeter (mm-) wave, or hybrid solutions. With free-space optics, Ref. [2] achieved 2.5Gbps over a 25km air-to-ground slant range in 2010. Similarly, Ref. [3] demonstrated up to 6Gbps data rate over an air-to-ground range of over 100 miles in 2015, using a hybrid mm-wave and free-space optics link. Recently, Facebook Connectivity also demonstrated a 100 Gbps optical link over a 10 km distance between a ground station and an air terminal [4].

In the mm-wave realm, Ref. [5] demonstrated 1Gbps data rate over a range of 40km, and Ref. [6] showed 20Gbps over a 1.7 km terrestrial link. Ref. [7] presents 40Gbps bi-directional link over a 16km terrestrial link. Ref [8] claimed 28-57Gbps over terrestrial links of up to 17km.

In this paper, we present test results of an E-band link between a fixed ground station and a Cessna aircraft. We also brief our experimental effort to spot-check the E-band rain loss model in a test campaign at Quillayute, WA. To the best of the authors' knowledge, this paper describes the world's first demonstration of a very high capacity mm-wave communication link system between a ground station and a fast-moving aerial platform over a significant range.

II. Link Budget and System Overview

A. Link Budget and System Block diagram

The E-band spectrum (71-86 GHz) was selected due to its sufficiently broad bandwidth and light spectrum regulation. The atmospheric attenuation at E-band is less than 1 dB/km in clear weather at sea level and decreases exponentially as the altitude increases. This is a big advantage for air-to-ground communication since most of the atmospheric loss exists in the first few kilometres near the ground. Fig. 1 shows the total atmospheric attenuation (TAA) values exceeded 97%, 99%, and 99.9% of the time for an Earth-to-air, zenith-pointing link in Los Angeles, according to the ITU-R P.618-12 model.

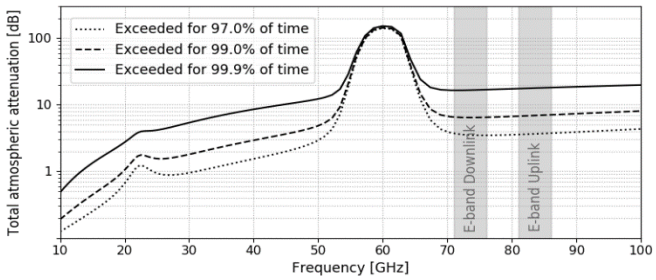

Fig. 1. Total atmospheric attenuation in Los Angeles (zenith pointing) for different time availabilities according to the ITU-R P.618-12 methodology.

The attenuation is greater at lower angles as the path travels through more atmosphere. With an elevation angle ranging

from 30° to 90°, the TAA for 90% of the time does not exceed 3.2 and 1.7dB (uplink and downlink, respectively), while the TAA is 12 and 7dB for 99%. For a HAP flying at an altitude of 90kft (27.4km) above the Los Angeles area, at a 30° elevation angle, the total path loss (free space path loss plus total atmospheric attenuation) is 174dB for 99% link availability.

Fig. 2 shows the block diagram of the ground terminal and the air payload, which were designed to meet the link budget requirements while achieving maximum throughput. The system can be further divided into the Communication (COM) and the Pointing, Acquisition, and Tracking (PAT) subsystems, which are described in the next two subsections.

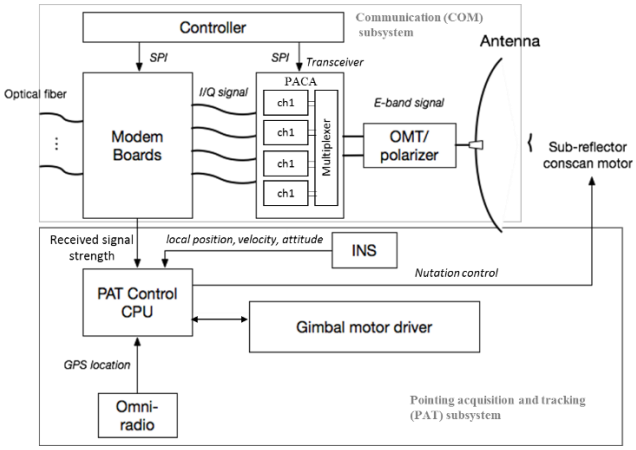

Fig. 2. System block diagram for the ground terminal / air payload.

B. COM Sub-system

The COM system includes the baseband modem, optical fiber interface, RF transceiver, multiplexer and polarizer, antenna, and data stream interfaces. The baseband modem essentially uses four commercial off-the-shelf Maxlinear 85110 ASICs. Each ASIC uses wideband single carrier QAM modulations (BPSK to 128QAM). The maximum data rate mode uses 128QAM with a symbol rate of 1.6Gsps, which yields an information rate of approximately 10Gbps from each ASIC. The transceiver system multiplexes 4 such 10Gbps modulated carriers to achieve the 40Gbps capability both in the uplink and downlink direction. The transceiver uses multiplexing both in spectrum and polarization. On the air-to-ground downlink 2 modulated carriers (72GHz and 75GHz) each with 2GHz bandwidth are aggregated using low insertion loss (<0.5dB) passive waveguide cavity filters after the power amplification stage. We refer to this technique as post amplification carrier aggregation (PACA). For the application of high capacity, long range, SWaP constrained link, PACA has a distinct advantages over the alternative approach of aggregating carriers before the power amplification stage. In the latter case the peak to average power ratio of the input signal to the power amplifier (PA) is high. This in turn results in PA to be backed off considerably from P_{1dB} for distortion-less operation which results in poor power efficiency. Two signals stream combined by the waveguide filters are simultaneously transmitted over RHCP and LHCP polarization by using an orthomode transducer and polarizer.

Commercial 8-way power combining GaAs PA is adopted with a saturation power (P_{sat}) of 33dBm and 31dBm P_{1dB}. The power combining efficiency is about 75%. The DC power consumption of each PA is 14W and its weight is 0.16 kg with heatsink. Digital predistortion (DPD) is applied to effectively increase power efficiency by reducing the transmit power back off. We have proven that DPD can push an extra 2-3dB of output power at E-band with a proper set of DPD coefficients [9]. For the antennas, the ground system adopts a 120cm meter axially displaced ellipse (ADE) dual-reflector antenna with a gain of 59dBi, whereas the airborne antenna is 18cm in diameter with a gain of 42dBi.

C. PAT Sub-system

The PAT system is in charge of the pointing, acquisition, and tracking of the antenna beam to and from the moving aircraft. It is composed of a gimbal, encoder, controller, inertial measurement unit (IMU), and a low-data-rate but highly-sustainable discovery link, which is responsible for communicating initial position acquisition, data logging, management, and control.

The ground antenna requires a pointing accuracy better than 0.05° which is equivalent to a 0.5dB loss. Notice that a 0.2° miss-pointing would be equivalent to 32dB of loss, since 0.2° is where the first null of the antenna pattern is located. Sources of pointing error include stabilization error, INS altitude error, INS position error, calibration and alignment error. Given the stringent pointing requirement, conical scanning (Conscan) is used to improve tracking: A spinning sub-reflector with a driving motor is mounted on the ground antenna for antenna beam nutation. The narrow beam is intentionally offset and nutated, which results in a received strength signal with sinusoidal shape, with period equal to the sub-reflector spinning period. The gimbal of the antenna is moved in the direction of the highest strength signal received. Conscan tracking aims to maximize the received power using a proportional–integral (PI) controller, which is part of the PAT Control CPU module.

Error offsets in the antenna boresight and the mount need to be calibrated before the flight test. There are 5 unknown parameters to be determined: pitch, yaw, and roll of the base, and elevation deviation and cross elevation deviation of the gimbal. The parameters are determined using a beacon with known position located 13km away from the terminal and by solar tracking.

Solar tracking is a reliable method for the ground antenna and mount boresight calibration, since the position of the sun is known precisely for any given location. By pointing the antenna at the sun, which rises about 3dB noise floor in contrast to the sky, and tracking its position for a period of time, we then work backwards to calculate the calibration offsets for the antenna and the mount. This method allows us to install and calibrate this system anywhere in the world. With a proper controller design and boresighting procedure, we can achieve RMS pointing errors < 0.02 degrees on the ground side.

III. Flight Demonstration

Fig. 3 shows a photo of our ground terminal and aerial payload. The aerial payload was mounted to the bottom of a

small Cessna aircraft, while the ground terminal was set-up on a rooftop. Several tests were conducted with different flight paths and system configurations to verify the performance of the overall system in terms of high precision pointing, link throughput and link availability.

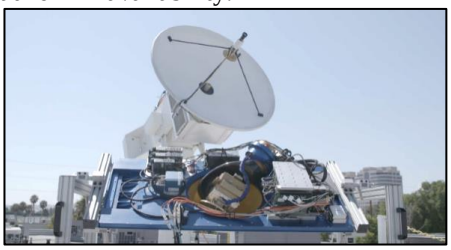

Fig. 3. A photo of the ground system (back) and the air payload (in front).

Fig. 4 depicts the flight path of one of the flight tests. The airplane flew at an altitude of 7km, with top speed of 463km/h. Flight tests were conducted at ground elevation angles ranging between 34° and 70° (the average elevation angle was 37°), whereas the slant range varied from 8.4 to 12km. At the ground terminal, we set the gimbal with a 40° blind zone in the azimuth plane, which is shown by the red-shadowed region of Fig. 4 (left). Whenever the airplane flew into the blind zone, the gimbal rotated back to the other side and waited for the airplane to come out of the blind zone. This was done to prevent twisting of the cables, but blind regions can be avoided by using cable slip rings.

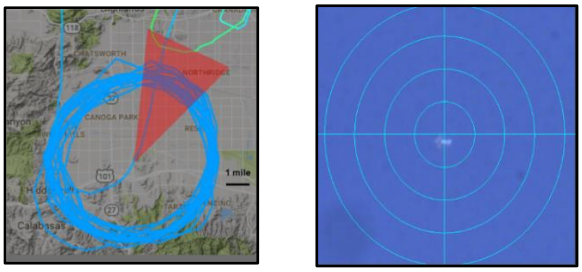

Fig. 4. (Left) the flight path of the airplane circling around the ground station, and (Right) a picture of the flying airplane seen through from a mounted camera co-aligned with the antenna axis to visualize the pointing performance.

The ground gimbal tracked the Cessna steadily, as monitored from the camera shown in Fig. 4 (right). Fig. 5 plots a histogram of the measured tracking error for the air and ground PAT systems during one of the test flights. Data in the y and z axes correspond to the tracking errors in the elevation and cross-elevation planes, respectively. As is shown, the air tracking accuracy was controlled to a precision of ±0.1°, whereas the ground Conscan tracking was controlled to ±0.02°. The air tracking doesn't need Conscan tracking because of its wider beamwidth.

Finally, Fig. 6 illustrates our test results for the data-rate at each channel in one of the test flights, measured through a third-party Ethernet traffic generator by Spirent Communications Inc. We achieved sustained data rates of 40Gbps downlink and 36Gbps uplink through the whole flight demonstration, with the uplink data rate peaking at 40Gbps. The bit-error-rate (BER) level ranged from 10^{-5} to 10^{-7} and varied according to channel performance. The data rate drops to 0 when the aircraft is in the blind zone.

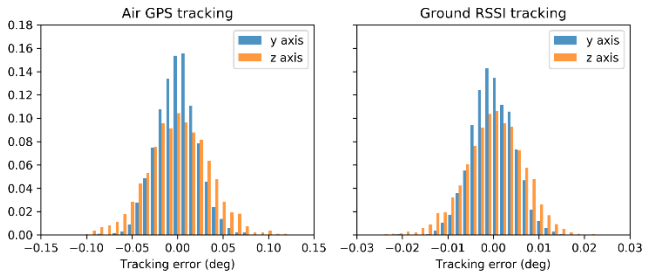

Fig. 5. Weighted-histogram of the tracking errors of the air and ground gimbal during the flight test.

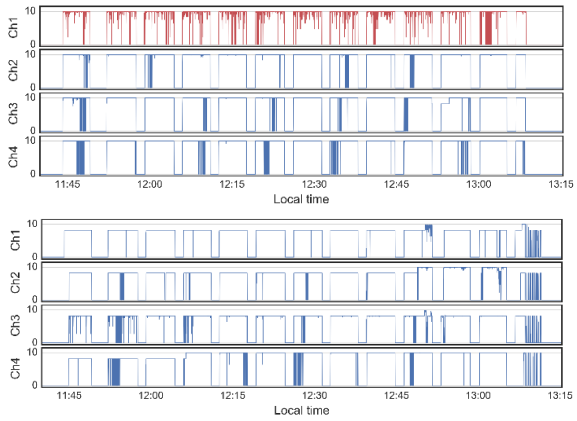

Fig. 6. Logged data rate for the air-to-ground downlink and ground-to-air uplink at each channel.

During the test flight, the Automatic Modulation and Coding (AMC) was turned off and the modulation for all channels was manually fixed to either 64QAM or 128QAM, which give 8Gbps or 10Gbps per channel respectively. Such setup was only for testing purposes. The link robustness can be easily improved by turning on the AMC. We observe Channel 1 in the downlink (colored in red) showing a wriggling data rate, which happened because the Error Vector Magnitude (EVM) of the channel 1 received signal was near the threshold of the BER limit, and the data rate drops to zero if the EVM is below that threshold. The main reason for the channel 1 EVM issue was the linearity of the transmitter which can be resolved by replacing one component in the Tx1 up-converter chain. All the other 3 channels, however, worked robustly at 10Gbps. The root cause of the 36Gbps uplink limit was the cross-polarization distortion (XPD) caused by suboptimal design of a circular waveguide spacer between the polarizer output and the antenna feed. In future versions this problem can be resolved.

IV. Flight Test For Rain Loss Model

Atmospheric attenuation for air-to-ground slant paths has been extensively studied in the past, in the context of satellite communications. The International Telecommunications Union (ITU) provides several methodologies within their Recommendations to estimate the gaseous (Rec. ITU-R P.676), clouds (Rec. ITU-R P.840), scintillation (Rec. ITU-R P.618), and rain (Rec. ITU-R P.618) contributions to the total atmospheric attenuation.

However, the ITU model for rain attenuation at slant paths (Rec. ITU-R P.618) is only recommended for links with

frequencies up to 55GHz. This is because the model was built empirically, using experimental data from links between geostationary satellites and ground stations, and the highest transmit frequency of such satellites was 55GHz. Therefore, in order to verify the atmospheric loss, in particular the rain and cloud attenuations at E-band, we conducted a test campaign at Quillayute airport (IATA designator UIL), located at coordinates 47.9358°N, 124.5619°W. Fifteen flights were performed over 9 days, starting on April 19, 2017.

While we recognize that such a short test campaign cannot claim to fully validate the statistical ITU models, these campaigns served to (a) spot-check the validity of these models when extrapolated beyond 55GHz (ensuring that there were no outlier values out-of-range), and (b) empirically measure the availability of our system under rain conditions.

The results of this test campaign (Fig. 7) show that for moderate rain conditions, 70% of the measured rain and cloud attenuation values fall within 2dB of that estimated using the ITU model. The rain attenuation is about 8dB for 99% link availability during rain episodes. We did not find any evidence that suggests that the ITU models are not valid. Indeed, we believe that the ITU-R P.618-12 model provides a good approximation for the rain attenuation measured during the test days, both at 73.5 and 83.5GHz, since most of the points fall within the region of error indicated by the ITU-R.

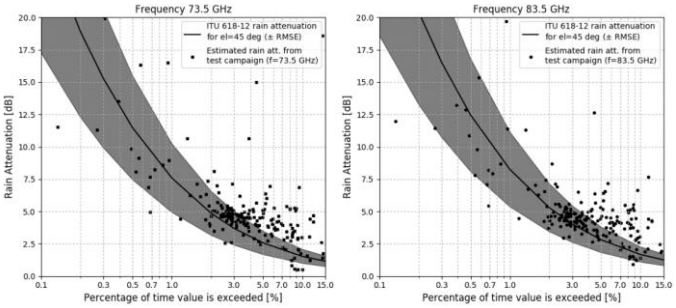

Fig. 7. Measured rain attenuation vs. values estimated by the ITU-R P.618-12 model.

Using the proven system performance and ITU path loss models, we estimated the achievable link distances, from a network deployment perspective. Fig. 8 shows the preliminary estimation of the achievable data rate as a function of flight altitude assuming the ground station located in Los Angeles, CA. The modulation schemes range from QPSK to 128QAM and the symbol rate is fixed to 1.6Gsps.

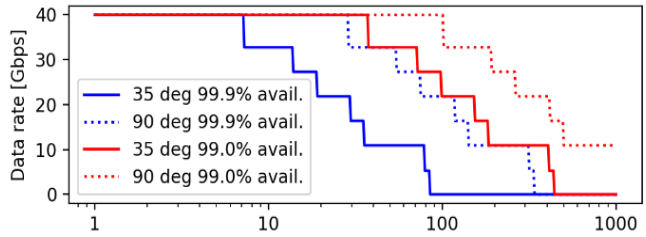

Fig. 8. Achievable data rate vs. flying altitude for different elevation angles and link availabilities.

A 40Gbps link can be sustained up to an altitude of 28km at 90° elevation angle (zenith) for a 99.9% availability, while a 10Gbps data rate link can be maintained for altitudes up to 310km in Los Angeles region. The results in the case of 99% availability and 35° elevation angle are also plotted in Fig. 8. Note that we haven't considered the impact of rain on the XPD degradation which can reduce the data rate especially at the high modulation scheme. Unfortunately, we didn't collect the data for polarization effect in Quillayute test.

V. Summary

We have designed, developed, and demonstrated a peak data rate of 40Gbps simultaneously in each direction via an air-to-ground link between a Cessna and a ground station with a slant range of up to 12km. With the plane flying at a top speed of 463km/h, the downlink data-rate was sustained at 40Gbps, whereas the uplink data-rate was sustained at 36Gbps, with peaks to 40Gbps for minutes at a time. The lower data rate in the uplink direction was due to the suboptimal axial ratio on the antenna feed; solving these issues in future revisions would allow us to achieve a truly robust 40Gbps bidirectional link. The system uses commercially available components. The total power consumption of the airborne link terminal was 363 Watts and the mass of the airborne terminal was measured at 11.8kg, while the ground terminal power consumption was 865 Watts. We also conducted test flights in Northwest Washington to spot check the ITU-R P.618-12 model for rain attenuation over an air-to-ground link and concluded that the collected rain attenuation data matches predictions of the ITU-R P.618-12 model.

References

[1] (2017) [Online]. Available: https://code.fb.com/connectivity/aquila-what-s-next-for-high-altitude-connectivity/

[2] Walther, Frederick G. et al. "Air-to-ground lasercom system demonstration design overview and results summary." FreeSpace Laser Communications, SPIE, 2010.

[3] D. W. Young, H. H. Hurt, J. E. Sluz and J. C. Juarez, "Development and Demonstration of Laser Communications Systems" , Johns Hopkins APL Technical Digest, Vol. 33, No. 2, 2015

[4] C. Chen, A. Grier, M. Malfa, E. Booen, H. Harding, C. Xia, M. Hunwardsen, J. Demers, K. Kudinov, G. Mak, B. Smith, A. Sahasrabudhe, F. Patawaran, T. Wang, A. Wang, C. Zhao, D. Leang, J. Gin, M. Lewis, B. Zhang, D. Nguyen, D. Jandrain, F. Haque, and K. Quirk, "Demonstration of a bidirectional coherent air-to-ground optical link," in Proc. SPIE, Free-Space Laser Communication and Atmospheric Propagation XXX, 2018

[5] R. Baker, B. Steagall, "Mobile Hotspots Millimeter Wave Communications" , Technical Panel: Millimeter Wave Technology Challenges and Trends in Defense and Commercial Applications, IEEE Military Communications Conference (MILCOM), 2017

[6] X. Li, J. Xiao, J. Yu, "Long-Distance Wireless mm-Wave Signal Delivery at W-Band", Journal of Lightwave Technology, vol. 34, no. 2, pp. 661-668, Jan, 2015.

[7] K. Brown, A. Brown, T. Feenstra, D. Gritters, E. Ko, S. O'Connor, M. Sotelo, "Long-range wireless link with fiber-equivalent data rate," 2017 IEEE MTT-S International Microwave Symposium (IMS), Honolulu, HI, 2017, pp. 809-811.

[8] T. Woodward, "The DARPA 100Gbp/s RF backbone program", National Science Foundation Millimeter-Wave Research Coordination Network (NSF mmW RCN) Workshop, 19 July, 2017.

[9] Q. Tang, H. Zhou, A. Tiwari, J. Stewart, Q. Qu, D. Zhang, H. Hemmati, "Experimental demonstration of digital pre-distortion for millimeter wave power amplifiers with GHz bandwidth", IEEE Radio and Wireless Week, March, Anaheim, CA, 2018.